Research Article

Di Jia, Cong Gao*, Yuliang Yang, Fuzhen Pang, Haichao Li, and Yuan Du

A semi-analytical method for dynamic analysis of a rectangular plate with general boundary conditions based on FSDT

https://doi.org/10.1515/rams-2022-0033 received December 15, 2021; accepted March 29, 2022

Abstract: In this paper, the unified Jacobi-Ritz method (JRM) is utilized to analyze the dynamic response of rectangular plates with general boundary conditions. First, the structural energy functional is established in the framework of the first-order shear deformation theory, and the rectangular plate is divided into several equal parts according to the domain decomposition method. Then, the artificial springs are introduced to ensure the continuity of segments and diversified boundary conditions. The Jacobi orthogonal polynomials are expanded to represent the displacement field in one direction. Finally, the free and forced vibration characteristics of the rectangular plate can be obtained by utilizing the Rayleigh-Ritz method, where the Newmark-β integration method is adopted to realize the time-domain solutions for transient vibration response. The results for different structural scale parameters and various boundary conditions are presented, and the validity and accuracy of the presented method are verified by comparing the results from published literature and FEM. The results of the study can provide technical support for vibration control of the plate structure.

Keywords: Jacobi polynomials, steady and transient vibration, rectangular plate, general boundary condition

1 Introduction

The rectangular plate structure has been widely used in practical engineering, which is usually subjected to various steady and transient loads. Therefore, an accurate analysis of the vibration characteristics of the rectangular plate can guide well its design in actual engineering applications.

In recent years, numerous studies have been conducted on the free and steady vibration of various structures, including the dynamic stiffness method [1], the separation variables method [2–4], the Ritz method [5–9], the generalized differential quadrature method [10], and the finite-element method (FEM) [11,12]. Yang et al. [13] carried out the exact solutions for the rectangular ceramic plate based on the 3D linear equations. Considering the influence of the initial stresses, Akbarov et al. [14] applied the 3D FEM to obtain the forced vibration response of the rectangular composite plate based on the 3D linearized theory. Wu et al. [15] studied the dynamic response of the rectangular plate under external load by applying the principle of mixed variables. Fan [16] performed the forced vibration of the rectangular plate by means of the damped complex modes analysis method. Based on the Hamilton variation principle, the research studies of Xiao and his colleagues [17-19] demonstrated the free and forced vibration characteristics of a thin rectangular plate on the nonlinear elastic foundation by using the Galerkin method. In the framework of Mindlin's first-order theory, Zhang et al. [20] illustrated the forced vibration characteristics of the rectangular piezoelectric plate, and the trigonometric series solutions were obtained under two types of boundary conditions. Nasirshoaibi and Mohammadi [21] applied the modal expansion method for vibration analysis of an elastically connected rectangular plate. According to the FSDT, a great deal of research studies on composite plates and shells were conducted by Shi et al. [9,22,23], who developed the improved Fourier series method, and the influences of boundary conditions and material

^{*} Corresponding author: Cong Gao, College of Shipbuilding Engineering, Harbin Engineering University, Harbin, 150001, People's Republic of China, e-mail: conggao@hrbeu.edu.cn, tel: +86-451-82589161

Di Jia: College of Power and Energy Engineering, Harbin Engineering University, Harbin, 150001, People's Republic of China; Naval Research Institute, Beijing, 100161, People's Republic of China Yuliang Yang, Fuzhen Pang, Haichao Li, Yuan Du: College of Shipbuilding Engineering, Harbin Engineering University, Harbin, 150001, People's Republic of China

parameters on the vibration characteristics of the structure were also discussed. Agarana and Ehigbochie [24] put to use the finite-difference method to analyze the dynamic response of the elastic orthotropic mindlin plate, and the results were compared with those obtained from the published literature. Yahnioglu and Yesi [25] extended the FEM to study the vibration characteristics of a thick composite plate based on the 3D linearized theory of elastic waves. More research studies on the steady vibration response of rectangular plates can be found in the literature [26–31].

With regard to the transient vibration, Ou and Mak [32] developed the time-domain FEM and BEM to investigate the transient vibration and sound radiation of the stiffened plate; the stiffeners can be located at any position inside the plate. Fan [33] obtained the transient vibration solutions of the rectangular plate under viscoelastic restraints by using the modal strain energy (method, and the vibration displacement function was approximately selected as a double infinite series. Geng et al. [34,35] dealt with the transient vibration response of an impacted plate by using the interpolated time-domain equivalent source method, and a steel ball impact experiment was carried out on the clamped rectangular steel plate to verify the effectiveness of the method. Considering the nonlinear effect, He and Kashiwagi [36] carried out the transient vibration response of the vertical plate under the impact of a pulse-type wave by using the full-nonlinear boundaryelement method. Based on von Karman's large deflection plate theory, Sheikh and Mukhopadhyay [37] investigated the transient vibration characteristics of stiffened plate structures by using the spline finite strip method, and the spline functions and finite-element shape functions represented the two direction displacement interpolation functions. Hajheidari and Mirdamadi [38] established the transient vibration analysis model of the laminated plate in the framework of the classical lamination plate theory, and the numerical solutions were obtained by using the spectral FEM. Skocilas et al. [39] carried out the transient vibration response of the thin plate with viscoelastic isotropic and anisotropic materials, in which the selected model was defined by applying the constitutive equations related to stress and deformation. Pang et al. [40] conducted a study on the safety of the platform deck structure caused by the transient impact load during the rocket launch process based on the FEM.

From the above analysis, the published literature have ample analysis ways for the steady vibration response of the rectangular plate; however, the research studies on the transient vibration response of rectangular plate structures are relatively lacking, particularly for damped transient attenuation vibration characteristics. Based on this background, this study aims at conducting the dynamic responses of rectangular plate structures subject to general boundary restraints based on the FSDT. The multi-segment principle and unified Jacobi orthogonal polynomials are introduced to ensure the convergence and effectiveness of the algorithm. Meanwhile, the dynamic response characteristics of the rectangular plate are parameterized research.

2 Mathematical formulation

2.1 Rectangular plate

Figure 1 shows the analytical model of rectangular plate, where a, b, and h represent the length, width, and thickness of the structure, respectively. The cartesian coordinate system (x, y, z) is adopted to describe the model, in which x, y, and z, respectively, represent the length, width, and thickness directions of the structure, u, v, and w, respectively, denote the displacement fields in the x-, y-, and z-directions of the middle surface. The rectangular plate boundary conditions can be obtained by introducing three groups of linear springs (k_u, k_v) , and k_w) and two groups of rotational springs (k_x) and k_y 0 at

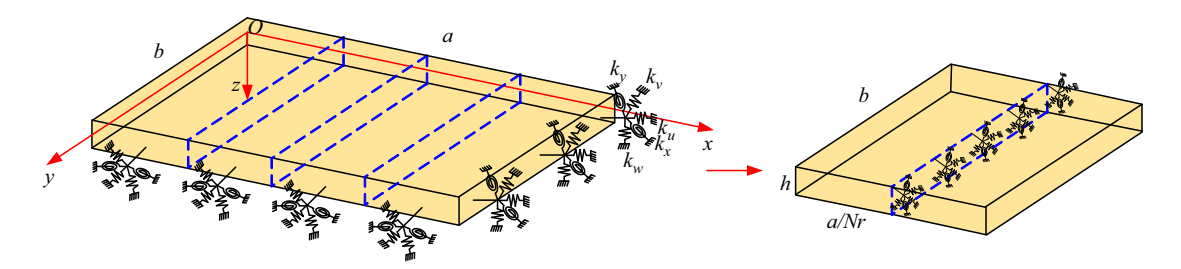


Figure 1: Calculation model of rectangular plate structure.

ends x = 0, x = a, y = 0, and y = b. Various boundary conditions can be simulated by setting different spring stiffness values. The rectangular plate is divided into H segments based on the DDM, where the ith segment is connected to the i + 1th segment by artificial springs. Normally, the stiffness of the connecting spring is set to infinity, indicating a direct strong coupling effect. Figure 2 exhibits the excitation point and the test point of the rectangular plate, and the load acts at the center of the structure in the z-direction. There are three vibration test points and one excitation point. The excitation point and test point are signified by first alphabet EP and TP, respectively, for subsequent analysis.

2.2 Expressions of rectangular plate's energy

The structural energy functional is established based on FSDT [41–43], and the assumed displacement field of the *i*th segment is expressed as

$$u^{i}(x, y, z, t) = u_{0}^{i}(x, y, t) + z\phi_{v}^{i}(x, y, t),$$
 (1a)

$$v^{i}(x, y, z, t) = v_{0}^{i}(x, y, t) + z\phi_{v}^{i}(x, y, t),$$
 (1b)

$$w^{i}(x, y, z, t) = w_{0}^{i}(x, y, t).$$
 (1c)

The strains of the rectangular plate are taken as follows:

$$\varepsilon_{xx}^i = \varepsilon_{xx}^{0,i} + z\chi_{xx}^i, \quad \varepsilon_{yy}^i = \varepsilon_{yy}^{0,i} + z\chi_{yy}^i,$$
 (2a)

$$y_{xy}^i = y_{xy}^{0,i} + z \chi_{xy}^i, \quad y_{yz}^i = y_{yz}^{0,i}, \quad y_{xz}^i = y_{xz}^{0,i},$$
 (2b)

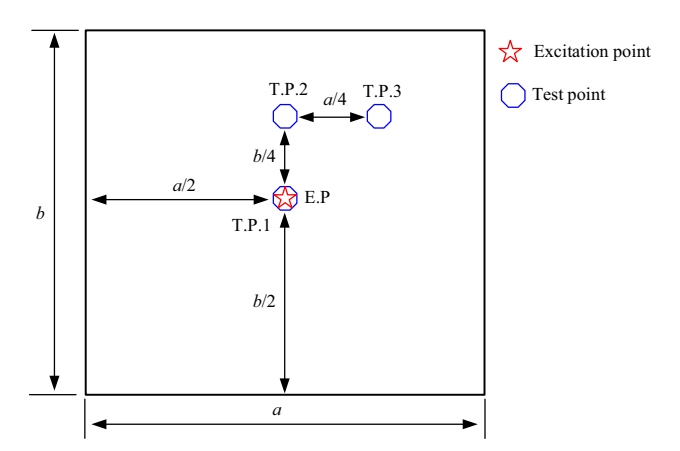


Figure 2: The excitation point and the examination point of the rectangular plate.

where ε_{xx}^i , ε_{yy}^i , γ_{xy}^i , γ_{yz}^i , and γ_{xz}^i , respectively, represent normal, shear, and transverse shear strains, and then,

$$\varepsilon_{xx}^{0,i} = \frac{\partial u_0^i}{\partial x}, \quad \varepsilon_{yy}^{0,i} = \frac{\partial v_0^i}{\partial y},$$
 (3a)

$$y_{xy}^{0,i} = \frac{\partial u_0^i}{\partial y} + \frac{\partial v_0^i}{\partial x}, \quad y_{yz}^{0,i} = \frac{\partial w_0^i}{\partial y} + \phi_y^i, \quad y_{xz}^{0,i} = \frac{\partial w_0^i}{\partial x} + \phi_x^i, \quad (3b)$$

$$\chi_{xx}^{i} = \frac{\partial \phi_{x}^{i}}{\partial x}, \quad \chi_{yy}^{i} = \frac{\partial \phi_{y}^{i}}{\partial y}, \quad \chi_{xy}^{i} = \frac{\partial \phi_{x}^{i}}{\partial y} + \frac{\partial \phi_{y}^{i}}{\partial x}.$$
 (3c)

The stress of the rectangular plate is shown as

$$\begin{pmatrix} \sigma_{xx}^{i} \\ \sigma_{yy}^{i} \\ \tau_{xy}^{i} \\ \tau_{yz}^{i} \\ \tau_{xz}^{i} \end{pmatrix} = \begin{bmatrix} Q_{11} & Q_{12} & 0 & 0 & 0 \\ Q_{12} & Q_{22} & 0 & 0 & 0 \\ 0 & 0 & Q_{66} & 0 & 0 \\ 0 & 0 & 0 & Q_{66} & 0 \\ 0 & 0 & 0 & 0 & Q_{66} \end{bmatrix} \begin{pmatrix} \varepsilon_{xx}^{i} \\ \varepsilon_{yy}^{i} \\ v_{xy}^{i} \\ v_{yz}^{i} \\ v_{yz}^{i} \\ v_{xz}^{i} \end{pmatrix},$$
 (4)

where σ_x^i , σ_y^i , τ_{xy}^i , τ_{xz}^i , and τ_{yz}^i , respectively, represent normal and shear stresses. Q_{ij} (i,j=1,2,6) can be expressed as

$$Q_{11} = Q_{22} = \frac{E}{1 - \mu^2}, \quad Q_{12} = \frac{\mu E}{1 - \mu^2}, \quad Q_{66} = \frac{E}{2[1 + \mu]},$$
 (5)

where E and μ represent elastic modulus and Poisson's ratio, respectively, and the forces and moments can be expressed as,

$$\begin{bmatrix}
N_{x}^{i} \\
N_{y}^{i} \\
N_{xy}^{i}
\end{bmatrix} = \int_{-h/2}^{h/2} \left\{\begin{matrix} \sigma_{xx} \\ \sigma_{yy} \\ \sigma_{xy} \end{matrix}\right\} dz, \begin{bmatrix}
M_{x}^{i} \\
M_{y}^{i} \\
M_{xy}^{i}
\end{bmatrix}$$

$$= \int_{-h/2}^{h/2} \left\{\begin{matrix} \sigma_{xx} \\ \sigma_{yy} \\ \sigma_{xy} \end{matrix}\right\} z dz, \begin{bmatrix}
Q_{xz}^{i} \\
Q_{yz}^{i}
\end{bmatrix} = \int_{-h/2}^{h/2} \bar{\kappa} \left\{\begin{matrix} \sigma_{xz} \\ \sigma_{yz} \\ \sigma_{yz} \end{matrix}\right\} dz. \tag{6}$$

The following equation can be obtained by substituting equation (4) into equation (6):

$$\begin{bmatrix} N_{xx}^{i} \\ N_{yy}^{i} \\ N_{xy}^{i} \\ M_{xx}^{i} \\ M_{yy}^{i} \\ M_{xy}^{i} \end{bmatrix} = \begin{bmatrix} A_{11} & A_{12} & 0 & B_{11} & B_{12} & 0 \\ A_{12} & A_{22} & 0 & B_{12} & B_{22} & 0 \\ 0 & 0 & A_{66} & 0 & 0 & B_{66} \\ B_{11} & B_{12} & 0 & D_{11} & D_{12} & 0 \\ B_{12} & B_{22} & 0 & D_{12} & D_{22} & 0 \\ 0 & 0 & B_{66} & 0 & 0 & D_{66} \end{bmatrix} \begin{bmatrix} \varepsilon_{xx}^{0,i} \\ \varepsilon_{yy}^{0,i} \\ \varepsilon_{yy}^{0,i} \\ \gamma_{xy}^{0,i} \\ \chi_{xx}^{i} \\ \chi_{yy}^{i} \\ \chi_{xy}^{i} \end{bmatrix}, (7a)$$

$$\begin{cases}
Q_x^i \\
Q_y^i
\end{cases} = \bar{\kappa} \begin{bmatrix} A_{55} & A_{45} \\ A_{45} & A_{44} \end{bmatrix} \begin{bmatrix} y_{xz}^{0,i} \\ y_{yz}^{0,i} \\ y_{yz}^{0,i} \end{bmatrix},$$
(7b)

where N_x , N_y , N_{xy} , M_x , M_y , M_{xy} , Q_{xz} , and Q_{yz} , respectively, represent the force, moment resultants, and transverse shear force of the structure, $\bar{\kappa}$ is the shear correction factor, and the value of the study is set as 5/6. A_{ij} , B_{ij} , and D_{ij} (i, j=1,2,6) are the extensional, extensional-bending coupling, and bending stiffness of the rectangular plate, which are shown as

$$(A_{ij}, B_{ij}, D_{ij}) = \int_{-h/2}^{h/2} Q_{ij}(1, z, z^2) dz.$$
 (8)

The strain energy is expressed as

$$U_{V}^{i} = \frac{1}{2} \int_{0}^{a} \int_{0}^{b} (N_{xx}^{i} \varepsilon_{xx}^{0,i} + N_{yy}^{i} \varepsilon_{yy}^{0,i} + N_{xy}^{i} \gamma_{xy}^{0,i} + M_{xx}^{i} \chi_{xx}^{i} + M_{xy}^{i} \chi_{yy}^{i} + M_{xy}^{i} \chi_{xy}^{i} + Q_{x}^{i} \gamma_{xz}^{0,i} + Q_{y}^{i} \gamma_{yz}^{0,i}) dx dy.$$

$$(9)$$

The following equation can be obtained by substituting equations (3) and (7) into equation (9)

$$U_{S}^{i} = \frac{1}{2} \int_{0}^{a} \int_{0}^{b} \left\{ A_{11} \left(\frac{\partial u_{0}^{i}}{\partial x} \right)^{2} + A_{22} \left(\frac{\partial v_{0}^{i}}{\partial y} \right)^{2} + A_{66} \left(\frac{\partial u_{0}^{i}}{\partial y} + \frac{\partial v_{0}^{i}}{\partial x} \right)^{2} + 2A_{12} \left(\frac{\partial u_{0}^{i}}{\partial x} \right) \left(\frac{\partial v_{0}^{i}}{\partial y} \right) + \bar{\kappa} A_{55} \left(\frac{\partial w_{0}^{i}}{\partial x} + \phi_{x}^{i} \right)^{2} + \bar{\kappa} A_{44} \left(\frac{\partial w_{0}^{i}}{\partial y} + \phi_{y}^{i} \right)^{2} + \bar{\kappa} A_{55} \left(\frac{\partial w_{0}^{i}}{\partial x} + \phi_{x}^{i} \right)^{2} + 2\bar{\kappa} A_{45} \left(\frac{\partial w_{0}^{i}}{\partial x} + \phi_{x}^{i} \right) \left(\frac{\partial w_{0}^{i}}{\partial y} + \phi_{y}^{i} \right) \right\}$$

 U_{BS}^i

$$= \frac{1}{2} \int_{0}^{a} \int_{0}^{b} \left\{ B_{11} \left(\frac{\partial u_{0}^{i}}{\partial x} \right) \left(\frac{\partial \phi_{x}^{i}}{\partial x} \right) + B_{12} \left[\left(\frac{\partial u_{0}^{i}}{\partial x} \right) \left(\frac{\partial \phi_{y}^{i}}{\partial y} \right) + \left(\frac{\partial v_{0}^{i}}{\partial y} \right) \left(\frac{\partial \phi_{x}^{i}}{\partial x} \right) \right] \right\}$$

$$+ B_{22} \left(\frac{\partial v_{0}^{i}}{\partial y} \right) \left(\frac{\partial \phi_{y}^{i}}{\partial y} \right) + B_{66} \left(\frac{\partial v_{0}^{i}}{\partial x} + \frac{\partial u_{0}^{i}}{\partial y} \right) \left(\frac{\partial \phi_{x}^{i}}{\partial y} + \frac{\partial \phi_{y}^{i}}{\partial x} \right) \right\}$$

$$dx dy.$$

$$(10b)$$

 $U_{B}^{i} = \frac{1}{2} \int_{0}^{a} \int_{0}^{b} \left\{ D_{11} \left(\frac{\partial \phi_{x}^{i}}{\partial x} \right)^{2} + 2D_{12} \left(\frac{\partial \phi_{x}^{i}}{\partial x} \right) \left(\frac{\partial \phi_{y}^{i}}{\partial y} \right) + D_{22} \left(\frac{\partial \phi_{y}^{i}}{\partial y} \right)^{2} + D_{66} \left(\frac{\partial \phi_{x}^{i}}{\partial y} + \frac{\partial \phi_{y}^{i}}{\partial x} \right) \right\} dx dy. \quad (10c)$

The boundary potential energy U_b for a rectangular plate is shown as

$$U_{b} = \frac{1}{2} \int_{0}^{b} \left\{ [k_{u,x0}u_{0}^{2} + k_{v,x0}v_{0}^{2} + k_{w,x0}w_{0}^{2} + k_{x,x0}\phi_{x}^{2} + k_{y,x0}\phi_{y}^{2}]_{x=0} \right\} dy$$

$$+ \left[k_{u,xL}u_{0}^{2} + k_{v,xL}v_{0}^{2} + k_{w,xL}w_{0}^{2} + k_{x,xL}\phi_{x}^{2} + k_{y,xL}\phi_{y}^{2}]_{x=a} \right\} dy$$

$$+ \frac{1}{2} \int_{0}^{a} \left\{ [k_{u,y0}u_{0}^{2} + k_{v,y0}v_{0}^{2} + k_{w,y0}w_{0}^{2} + k_{x,y0}\phi_{x}^{2} + k_{y,y0}\phi_{y}^{2}]_{y=0} \right\} dx.$$

$$(11)$$

The potential energy of the connective spring is given by

 U_c^i

$$= \frac{1}{2} \int_{0}^{b} \begin{cases} k_{u}(u_{0}^{i} - u_{0}^{i+1})^{2} + k_{v}(v_{0}^{i} - v_{0}^{i+1})^{2} \\ + k_{w}(w_{0}^{i} - w_{0}^{i+1})^{2} \\ + k_{x}(\phi_{x}^{i} - \phi_{x}^{i+1})^{2} + k_{y}(\phi_{y}^{i} - \phi_{y}^{i+1})^{2} \end{cases}_{i,i+1} dy.$$
 (12)

The total potential energy is expressed as

$$U_{BS} = U_b + \sum_{i=1}^{H-1} U_s^i.$$
 (13)

The kinetic energy of the *i*th segment is shown as below

$$T^{i} = \frac{1}{2} \int_{0}^{a} \int_{0}^{b} \left\{ I_{1} \left[\left(\frac{\partial u_{0}^{i}}{\partial t} \right)^{2} + \left(\frac{\partial v_{0}^{i}}{\partial t} \right)^{2} + \left(\frac{\partial w_{0}^{i}}{\partial t} \right)^{2} \right] + I_{3} \left[\left(\frac{\partial \phi_{x}^{i}}{\partial t} \right)^{2} + \left(\frac{\partial \phi_{y}^{i}}{\partial t} \right)^{2} \right] + 2I_{2} \left[\left(\frac{\partial u_{0}^{i}}{\partial t} \right) \left(\frac{\partial \phi_{x}^{i}}{\partial t} \right) + \left(\frac{\partial v_{0}^{i}}{\partial t} \right) \left(\frac{\partial \phi_{y}^{i}}{\partial t} \right) \right] \right\} dxdy, \quad (14)$$

where

$$(I_1, I_2, I_3) = \int_{-h/2}^{h/2} \rho(1, z, z^2) dz.$$
 (15)

The work done by the external concentrated load on the *i*th rectangular plate segment is

$$W^{i} = \int f_{w,i} w_{i} \mathrm{d}x, \tag{16}$$

where $f_{w,i}$ is the external concentrated load inflicted in the *z*-direction.

2.3 The displacement function and the characteristic equation of the system

Based on the multi-segment partitioning principle, the Jacobi orthogonal polynomials [44–46] are expanded to represent the displacement field in one direction. The recurrence formulas of Jacobi polynomials are derived as

$$P_0^{(\alpha,\beta)}(\phi) = 1, \tag{17a}$$

$$P_1^{(\alpha,\beta)}(\phi) = \frac{\alpha + \beta + 2}{2}\phi - \frac{\alpha - \beta}{2},\tag{17b}$$

$$P_{i}^{(\alpha,\beta)}(\phi) = \frac{(\alpha + \beta + 2i - 1)\{\alpha^{2} - \beta^{2} + \phi(\alpha + \beta + 2i)(\alpha + \beta + 2i - 2)\}}{2i(\alpha + \beta + i)(\alpha + \beta + 2i - 2)} \times P_{i-1}^{(\alpha,\beta)}(\phi) - \frac{(\alpha + i - 1)(\beta + i - 1)(\alpha + \beta + 2i)}{i(\alpha + \beta + i)(\alpha + \beta + 2i - 2)} P_{i-2}^{(\alpha,\beta)}(\phi),$$
(17c)

where $\phi \in [-1, 1]$, $\alpha, \beta > -1$, and i = 2, 3, ...

Each of the displacement function components of the plate is written in the form of Jacobi polynomials and trigonometric series as follows:

$$u_0 = \sum_{m=0}^{M} \sum_{n=0}^{N} A_m P_m^{(\alpha,\beta)}(x) \cos\left(\frac{n\pi y}{b}\right) e^{i\omega t}, \quad (18a)$$

$$v_0 = \sum_{m=0}^{M} \sum_{n=0}^{N} B_m P_m^{(\alpha,\beta)}(x) \sin\left(\frac{n\pi y}{b}\right) e^{i\omega t}, \quad (18b)$$

$$w_0 = \sum_{m=0}^{M} \sum_{n=0}^{N} C_m P_m^{(\alpha,\beta)}(x) \sin\left(\frac{n\pi y}{b}\right) e^{i\omega t}, \quad (18c)$$

$$\phi_{x} = \sum_{m=0}^{M} \sum_{n=0}^{N} D_{m} P_{m}^{(\alpha,\beta)}(x) \sin\left(\frac{n\pi y}{b}\right) e^{i\omega t}, \quad (18d)$$

$$\phi_{y} = \sum_{m=0}^{M} \sum_{n=0}^{N} E_{m} P_{m}^{(\alpha,\beta)}(x) \cos\left(\frac{n\pi y}{b}\right) e^{i\omega t}, \quad (18e)$$

where A_m , B_m , C_m , D_m , and E_m indicates the expansion coefficients.

The Lagrangian energy function of a rectangular plate is given by

$$\mathcal{L} = \sum_{i=1}^{N-1} (W^{i} + T^{i} - U_{V}^{i}) - U_{BS}.$$
 (19)

Minimizing the energy function with respect to unknown expansion coefficients

$$\frac{\partial \mathcal{L}}{\partial \theta} = 0$$
, $\theta = A_m$, B_m , C_m , D_m , E_m . (20)

Therefore, the dynamic response equation of rectangular plate is derived as

$$(\mathbf{K} - \boldsymbol{\omega}^2 \mathbf{M}) \mathbf{Q} = \mathbf{F},\tag{21}$$

where K, M, and Q respectively signify the stiffness, mass, and coefficients matrix. By solving equation (21), the free vibration results for the rectangular plate can be obtained.

2.4 Vibration response solution

The unknown coefficients matrix of the rectangular plate under external excitation is derived as

$$\mathbf{0} = (\mathbf{K} - \boldsymbol{\omega}^2 \mathbf{M})^{-1} \mathbf{F}.$$
 (22)

where F denote the external excitation matrix, and the steady forced vibration response of rectangular plate can be obtained by substituting the above results into equa-

The Rayleigh damping is used in this study

$$\mathbf{C} = a\mathbf{M} + b\mathbf{K},\tag{23}$$

where **C** denotes the damping matrix, a and b are denoted as follows:

$$a = \frac{2w_i w_j}{w_i + w_j} \xi, b = \frac{2\xi}{w_i + w_j},$$
 (24)

where w_i and w_i denote the *i*th and *j*th frequency of the structure and ξ is the damping ratio. The Rayleigh damping is set as a = 2, b = 0.00003 in this study.

Assuming that the acceleration is constant within the time range of $[t, t + \Delta t]$, two parameters β and y are introduced at the same time:

$$\Delta \dot{x}_i = [(1 - \beta)\ddot{x}_i + \beta \ddot{x}_{i+1}]\Delta t, \qquad (25a)$$

$$\Delta x_i = \dot{x}_i \Delta t + \left[\left(\frac{1}{2} - \gamma \right) \ddot{x}_i + \gamma \ddot{x}_{i+1} \right] \Delta t^2.$$
 (25b)

In this study, $\beta = 1/2$, $\gamma = 1/4$, and the above formula can be solved to obtain

$$\ddot{x}_{i+1} = \frac{1}{\gamma \Delta t^2} \Delta x_i - \frac{1}{\gamma \Delta t} \dot{x}_i - \left(\frac{1}{2\gamma} - 1\right) \ddot{x}_i, \quad (26a)$$

$$\dot{x}_{i+1} = \frac{\beta}{\gamma \Delta t} \Delta x_i - \left(1 - \frac{\beta}{\gamma}\right) \dot{x}_i + \left(1 - \frac{\beta}{2\gamma}\right) \ddot{x}_i \Delta t. \quad (26b)$$

The incremental balance equation is shown as

$$M\ddot{x}_{i+1} + C\dot{x}_{i+1} + Kx_{i+1} = F_{i+1}.$$
 (27)

Substituting equation (26) into equation (27) can be obtained

$$[\overline{K}]x_{i+1} = \overline{F}_{i+1}. (28)$$

where

$$[\overline{K}] = K + \frac{1}{\gamma \Delta t^2} M + \frac{\beta}{\gamma \Delta t} C,$$
 (29)

$$\bar{F}_{i+1} = F_{i+1} + M \left(\frac{1}{\gamma \Delta t^2} x_i + \frac{1}{\gamma \Delta t} \dot{x}_i + \left(\frac{1}{2\gamma} - 1 \right) \ddot{x}_i \right) + C \left(\frac{\beta}{\gamma \Delta t} x_i + \left(\frac{\beta}{\gamma} - 1 \right) \dot{x}_i + \left(\frac{\beta}{2\gamma} - 1 \right) \ddot{x}_i \Delta t \right).$$
(30)

The response of the structure at any time can be obtained by repeating the iteration until the end of the time.

3 Validation and discussion

The free, clamped, simply support, and elasticity support boundary conditions are signified by F, C, S, and E, respectively. Unless otherwise indicated, the geometrical dimensions and material properties in this study are as follows: a = 1 m, b = 1 m, h = 0.05 m; E = 210 GPa, $\rho = 7,800 \text{ kg·m}^{-3}$, $\mu = 0.3$; M = 8, $\alpha = 1$, $\beta = 1$, H = 6. The nondimensional frequency is defined as $\Omega = \omega b^2/\pi^2 \sqrt{\rho h/D}$.

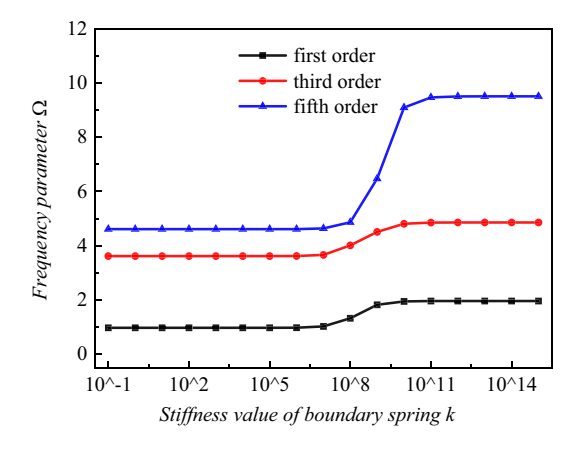
3.1 Convergence study

Combined with the specific conditions of simply supported square plates on four sides, the convergence of the method is discussed. It is worth noting that the following conclusions are also valid for rectangular plates with other boundary conditions. As mentioned earlier, the artificial springs and DDM are utilized in the proposed method; therefore, the convergence of the algorithm depends on the spring stiffness, Jacobi parameters, and the number of segments.

The frequency parameters of rectangular plates with different spring stiffnesses are shown in Figure 3. As the spring stiffness changes in the range of 10^{-1} – 10^{15} , the boundary conditions and continuity conditions change from free state to clamped state. Obviously, the stiffness value can be selected as zero for the free boundary condition, and the stiffness values can be selected in the range of 10^{12} – 10^{15} for the clamped boundary condition. Whether its a boundary spring or the connective spring, the dimensionless frequency parameter obviously increases rapidly, with the spring value increasing in the range of 10⁶-10¹⁰. The boundary conditions of the plate used in this paper are shown in Table 1 [47,48]. It should be noted that although different coupling and boundary conditions can be easily simulated by adjusting the stiffness of the artificial springs, modeling rigid constraints with high stiffness values may generate boundless results [49,50]; the penalty method with negative stiffness can be used to determine the appropriate stiffness to obtain accurate results.

Figure 4 exhibits the variation of the dimensionless results for a different number of segments and the highest order of the Jacobi polynomial. As expected, the frequency parameters stable quickly when $H \ge 3$ and $M \ge 4$. However, the matrix pathological can be obtained if the convergence parameters are too large. Therefore, the number of segments H is chosen as 6, and the polynomial truncation number M is selected as 8 in this study.

As mentioned earlier, the Jacobi polynomial can be transformed into the Chebyshev polynomial or the Legendre polynomial by selecting different values of Jacobi parameters. The relative percentage errors of rectangular plates with different Jacobi parameters are shown in Figure 5, and $\alpha=\beta=1$ is selected as the



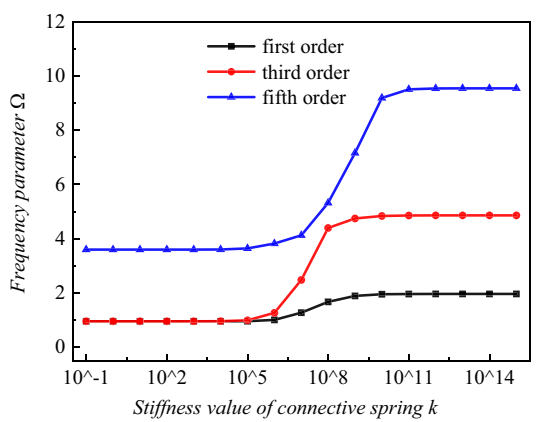


Figure 3: Frequency parameters Ω of rectangular plate with different boundary parameters.

reference value. Obviously, the maximum relative percentage error is almost negligible in the existing method regardless of the values of α and β , which means that the introduction of the Jacobi polynomial enriches the selection and diversity of displacement functions.

3.2 Free vibration characteristics of the rectangular plate

In this section, the free vibration solutions of the rectangular plate under general boundary constraints are compared with the existing literature. Table 2 shows the comparison of dimensionless frequency parameters between the proposed method and the published literature [51]. The comparison study indicates that the current method has higher accuracy for free vibration analysis of the rectangular plate. Figure 6 displays the mode shape of a rectangular plate; it is apparent that the proposed method in this paper can well display the mode shapes of the rectangular plate under general boundary conditions.

Table 3 and Figure 7 show the dimensionless frequency parameters of a rectangular plate with different shear correction factors under general boundary restraints.

Table 1: The spring stiffness values of the general edge conditions

Boundary conditions	k _u	k_{ν}	k _w	k _x	k _y
F	0	0	0	0	0
E	10 ⁸				
S	10 ¹⁵	10 ¹⁵	10 ¹⁵	0	0
C	10 ¹⁵				

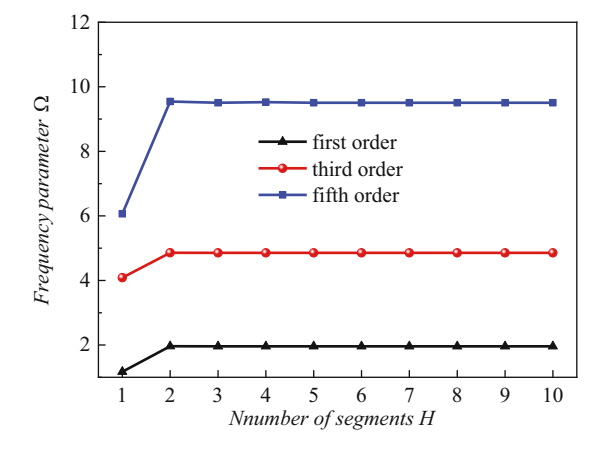
It is not hard to find that the shear correction factor has little influence on the dimensionless frequency parameters. At the same time, the boundary constraint has a significant impact on the vibration characteristics of the rectangular plate, and the frequency parameter gradually increases with the enhancement of the boundary conditions, which means that the enhancement of the boundary conditions increases the overall stiffness of the structure.

Table 4 and Figure 8 display the dimensionless frequency parameters of the rectangular plate with various a/b ratios under general boundary restraints. The results indicate that the nondimensional frequency parameters gradually decrease in general with the a/b ratio increase. That is to say, when the width (b) of the rectangular plate is fixed, the overall stiffness of the structure gradually decreases as the length (a) increases.

3.3 Steady vibration characteristics of the rectangular plate

In this section, the steady forced vibration analysis of the rectangular plate subjected to external excitation load is carried out. The excitation load is the unit concentrated force along the z-direction, the analysis frequency band is from 2 to 1,000 Hz, and the interval is 2 Hz.

Figure 9 displays the comparison results for the steady vibration response of the present method and FEM. Obviously, the proposed method is in good agreement with the FEM results, and the trends of the two curves are basically the same; there is only a small deviation at the single peak. In other words, the current



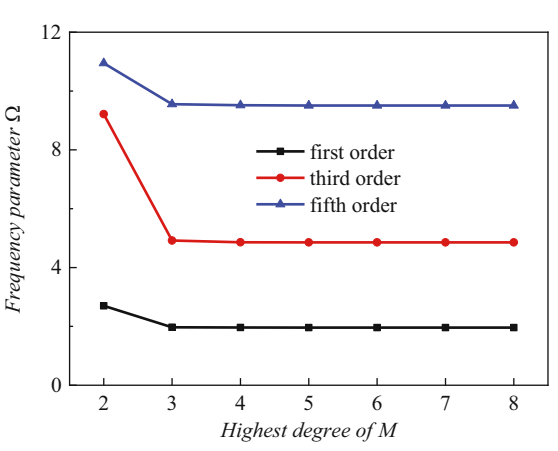


Figure 4: Frequency parameters $\boldsymbol{\Omega}$ of rectangular plate with different convergence parameters.

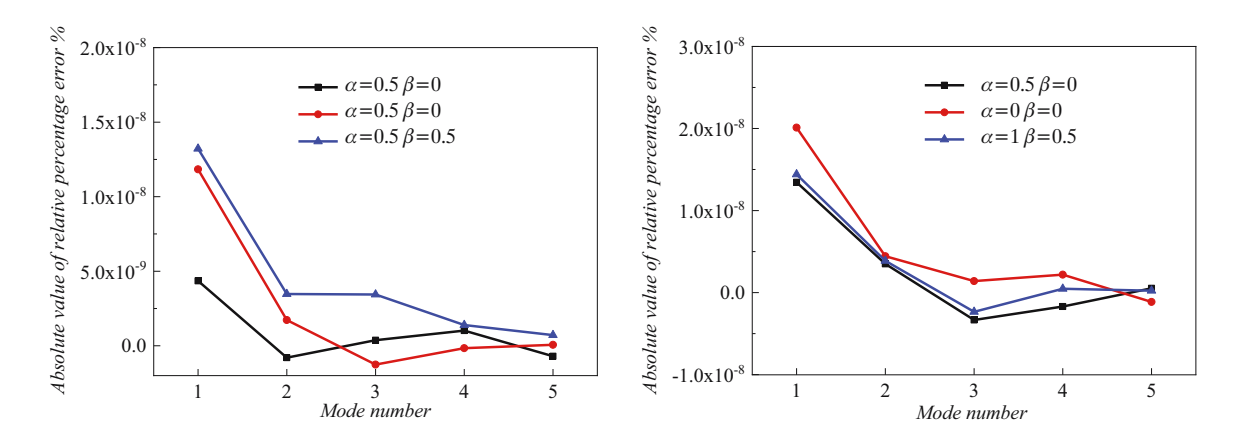


Figure 5: Relative percentage error of rectangular plate with different Jacobi parameters.

Table 2: Comparison of the natural frequency of present method and published literature

Boundary conditions		SSSS		SSSC		CSCS	
	Mode.no	Ref. [51]	Present	Ref. [51]	Present	Ref. [51]	Present
a/b = 0.4	1	7.2500	7.2494	7.4410	7.4447	7.6842	7.6863
	2	10.2500	10.2482	10.8840	10.8832	11.6290	11.6299
	3	15.2500	15.2472	16.4120	16.4167	17.7090	17.7157
	4	22.2490	22.2462	23.9560	23.9567	25.8040	25.8022
	5	25.9990	25.9981	26.0930	26.0977	26.2020	26.2064
a/b = 0.6	1	3.7780	3.7775	4.0540	4.0604	4.4270	4.4310
	2	6.7780	6.7772	7.5750	7.5700	8.5095	8.5052
	3	11.7780	11.7769	12.2540	12.2515	12.4280	12.4219
	4	12.1110	12.1106	13.1200	13.1131	14.6050	14.6161
	5	15.1110	15.1098	15.6220	15.6236	16.2170	16.2180

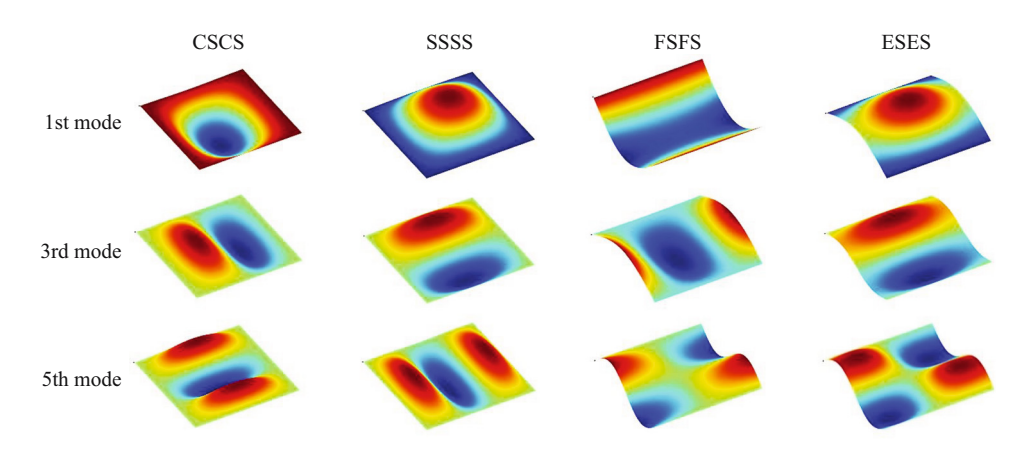


Figure 6: The mode shape of rectangular plate.

approach can effectively analyze the steady vibration of the rectangular plate.

After verifying the effectiveness of the proposed method for the steady forced vibration of the rectangular plate, a parametric study on the steady vibration characteristics of the rectangular plate is presented. First, Figure 10 shows the comparison results for the steady vibration response of the rectangular plate under various boundary conditions. The results indicate that the boundary conditions have a significant influence on the steady vibration

Table 3: Nondimensional frequency parameters of rectangular plate subject to general boundary conditions

CSCS Mode.no SSSS **FSFS ESES CSFS** $\kappa = 3/6$ 1 2.8321 1.9450 0.9677 1.8392 1.2649 5.2943 2 4 7939 1 5970 3 1285 3 2270 3 6.5499 4 7949 3 5849 4 6285 4 0913 4 8.8248 7.4947 3.8355 5.3910 6.0497 5 9.6420 9.3375 4.5561 6.3000 6.8901 $\kappa = 4/6$ 2.8547 1.9542 0.9692 1.8753 1.2687 2 5.3465 4.8322 1.6029 3.2055 3.2498 3 6.6503 3.6058 4.8331 4.6904 4.1175 4 8.9775 7.5860 3.8574 5,4840 6.1128 5 9.7823 9,4634 4.5889 6.4489 6.9747 $\kappa = 5/6$ 1 2.8685 1.9601 0.9702 1.9023 1.2710 2 5.3789 4.8561 1.6067 3.2643 3.2641 3 6.7130 4.8569 3.6191 4.7326 4.1336 4 9.0738 7.6436 3.8708 6.1523 5.5526 5 9.8699 9 5420 4 6094 6.5559 7 0275 1 $\kappa = 1$ 2.8779 1.9642 0.9709 1.9237 1.2727 2 5.4009 4.8725 1.6093 3.3118 3,2739 3 6.7558 4.1446 4.8733 3.6285 4.7638 4 9.1400 7.6834 3.8799 5.6066 6.1795 9.9298 9.5958 4.6234 6.6381 7.0636

response of the structure. In addition, the first peak frequency of the steady vibration gradually increases with the increase of the boundary conditions, while the number of peaks gradually decreases. At the same time, it is not difficult to find that the peak of the steady vibration appears at the natural frequency of the rectangular plate. It can be concluded that the natural frequency of the structure gradually increases with the enhancement of boundary conditions, while the number of natural frequencies of the structure within a certain frequency range decrease.

Figures 11–12 show the comparison results for the steady vibration characteristics of the rectangular plate with different h/a and a/b ratios. The results demonstrate that the first peak frequency gradually increases with

Table 4: Nondimensional frequency parameters of rectangular plate with different a/b radio

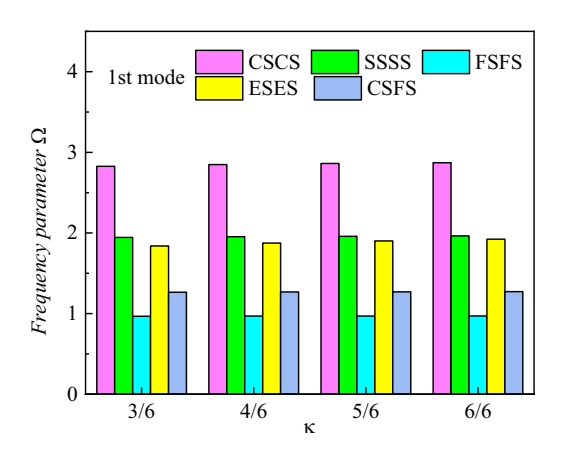
	Mode.no	cscs	SSSS	FSFS	ESES	CSFS
a/b = 0.5	1	8.9615	4.8231	0.9582	2.8350	2.2526
	2	10.8082	7.5613	2.6810	5.9866	4.9644
	3	14.4478	12.0863	3.8261	6.0269	9.4592
	4	19.9047	15.7744	6.2370	10.0635	9.5061
	5	22.1490	18.1974	8.4869	10.7104	12.3241
a/b = 1	1	2.8685	1.9601	0.9702	1.9023	1.2710
	2	5.3789	4.8561	1.6067	3.2643	3.2641
	3	6.7130	4.8569	3.6191	4.7326	4.1336
	4	9.0738	7.6436	3.8708	5.5526	6.1523
	5	9.8699	9.5420	4.6094	6.5559	7.0275
a/b = 2	1	1.3756	1.2385	0.9812	1.2771	1.0497
	2	2.3614	1.9711	1.1739	1.9323	1.5786
	3	3.8323	3.1883	1.7673	2.7605	2.5689
	4	4.2299	4.1654	2.7593	3.8094	3.9586
	5	5.1036	4.8734	3.8973	4.1584	4.0161

increasing h/a ratio, which indicates that the increase of thickness of the rectangular plate has an obvious influence on the structural stiffness. In addition, the first peak frequency of the structure gradually decreases as the length (a) increases when the width (b) of the rectangular plate is fixed, while the number of peaks within a certain frequency range increases, which is consistent with the conclusion of free vibration.

3.4 Transient vibration characteristics of rectangular plate

For transient vibration response, three different types of time-dependent loads are considered in the paper, which is shown in Figure 13.

(a) Rectangular pulse load



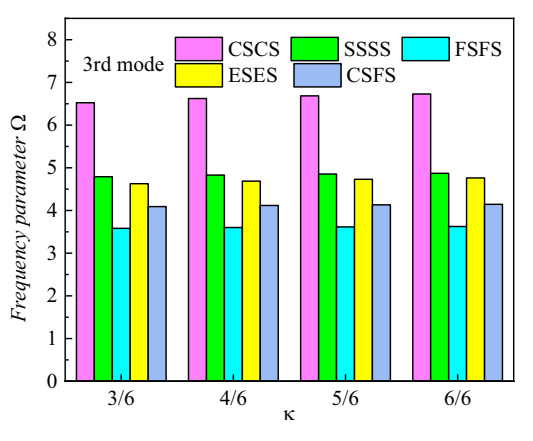


Figure 7: Frequency parameters Ω of rectangular plate with different shear correction factors.

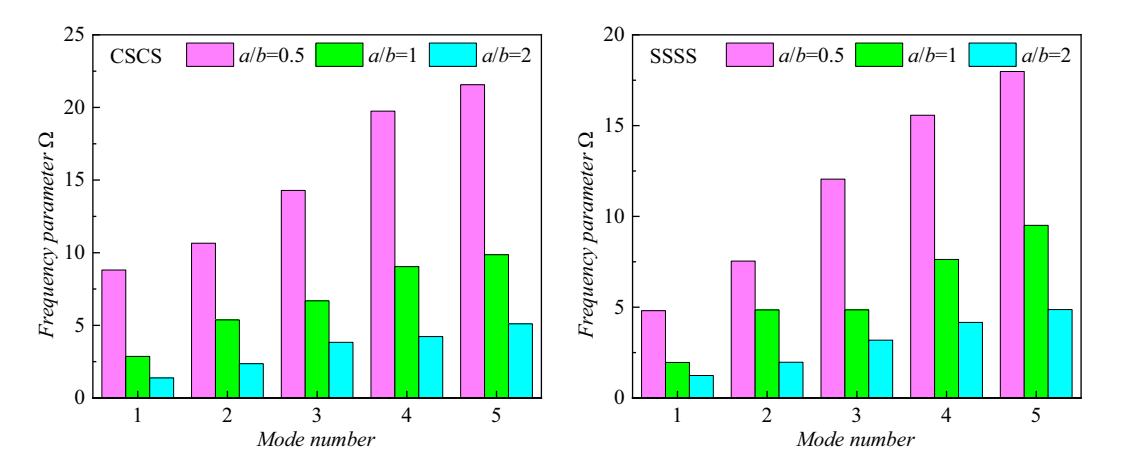


Figure 8: Frequency parameters Ω of rectangular plate with different a/b ratio.

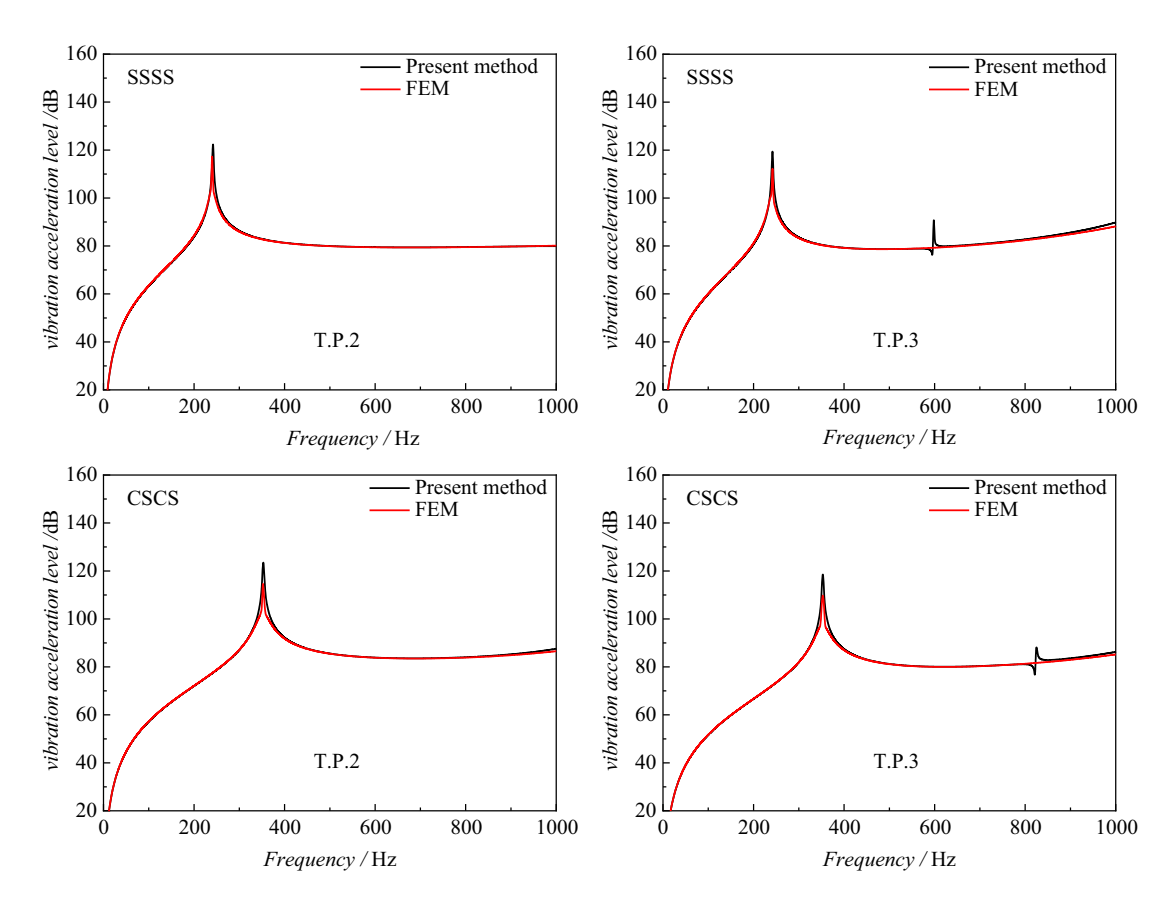


Figure 9: Comparison of the steady vibration response of the present method and FEM results.

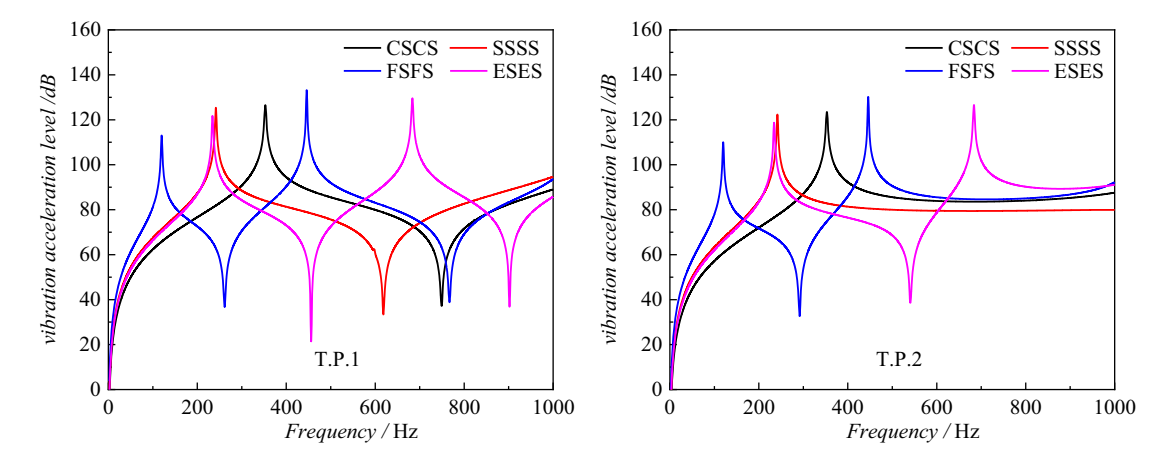


Figure 10: Comparison of the steady vibration of rectangular plate with different boundary conditions.

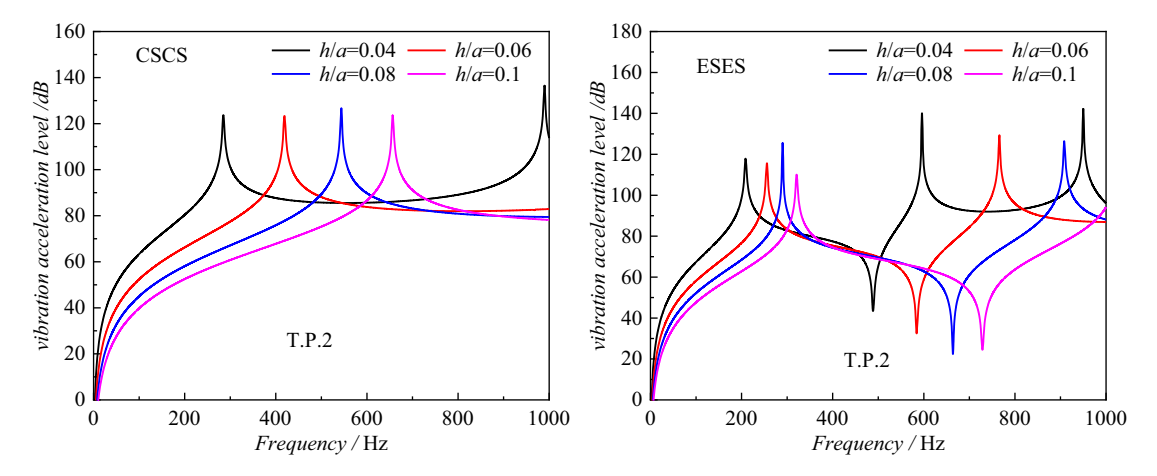


Figure 11: Comparison of the steady vibration of rectangular plate with different h/a ratios.

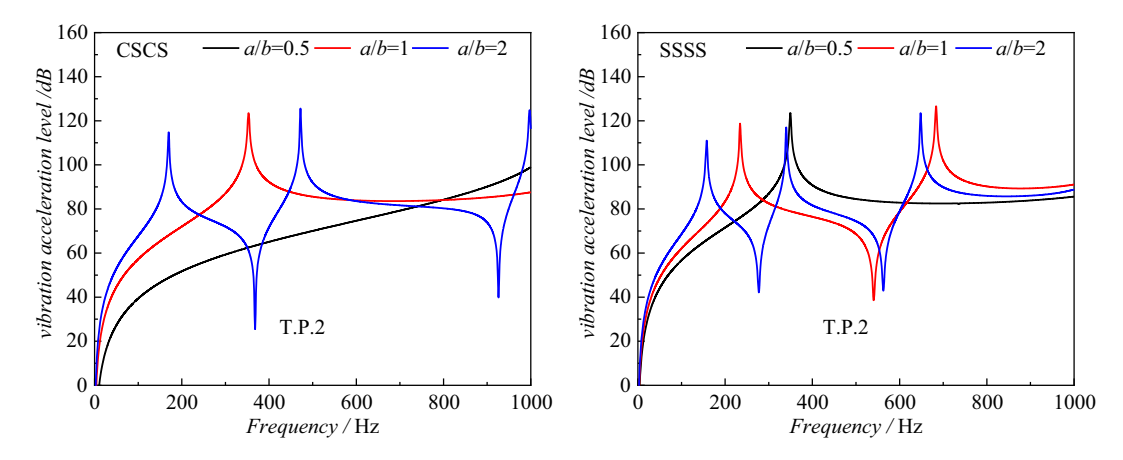


Figure 12: Comparison of the steady vibration of rectangular plate with different a/b radios.

$$f(t) = \begin{cases} q_0, & t_0 \le t \le t_0 + \tau \\ 0 & \end{cases}$$
 (31)

(b) Sine pulse load

Sine pulse load
$$f(t) = \begin{cases} q_0 \star \sin\left(\frac{\pi}{\tau} \star t - \frac{\pi}{\tau} \star t_0\right), & t_0 \le t \le t_0 + \frac{\tau}{2} \\ q_0 \star \sin\left(-\frac{\pi}{\tau} \star t + \frac{\pi}{\tau} \star t_0\right), & t_0 + \frac{\tau}{2} \le t \le t_0 + \tau \\ + \pi, & t_0 \end{cases}$$

(c) Triangular pulse load

$$f(t) = \begin{cases} q_0 \left(\frac{2}{\tau} \star t - \frac{2}{\tau} \star t_0\right), t_0 \le t \le t_0 + \frac{\tau}{2} \\ q_0 \left(-\frac{2}{\tau} \star t + \frac{2}{\tau} \star t_0 + 2\right), t_0 + \frac{\tau}{2} \le t \le t_0 + \tau \end{cases}$$
(33)

First, the transient response analysis of the undamped system is carried out. Figure 14 displays comparison results for the undamped transient vibration response of present method and FEM under rectangular pulse load, in which $q_0 = 1 \text{ N}$, $t_0 = 0.005 \text{ s}$, $\tau = 0.005 \text{ s}$, $\Delta t = 0.005 \text{ s}$ 0.0001 s. Obviously, the proposed method is in good agreement with the FEM calculation results, and the trends of the two curves are basically the same; in other words, the present method can effectively analyze the transient vibration response for the rectangular plate.

Figure 15 displays the comparison of the undamped transient vibration with different boundary conditions under a rectangular plate. The amplitude of the undamped vibration response increases with the weakening of boundary conditions. Undoubtedly, the weakening of boundary conditions reduces the stiffness of the structure and makes the structure more prone to vibration. Then, the comparison of the undamped transient vibration with different types of time-dependent loads under different boundary conditions is shown in Figure 16, and the vibration pickup points are chosen as point 2; the action time and amplitude of those three kinds of loads are precisely the same. The influence of the rectangular pulse load on the structure is always more significant than that of sine pulse load and triangular pulse load from the perspective of the amplitude of the displacement response at the initial moment of load application.

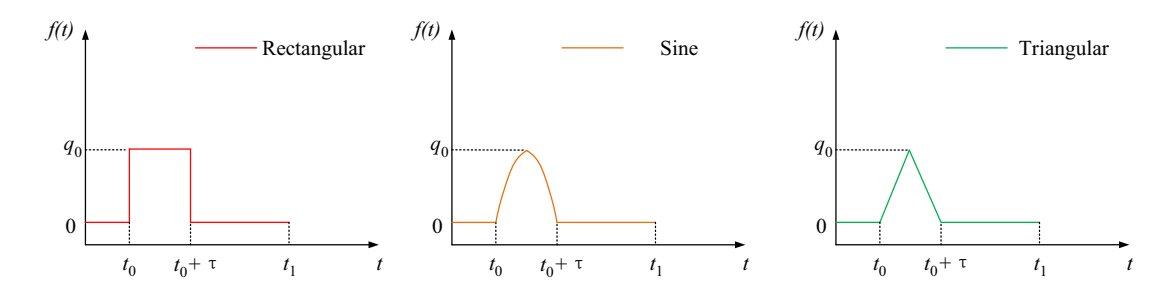


Figure 13: Sketch of applied load for rectangular plate with three different types of time-dependent loads.

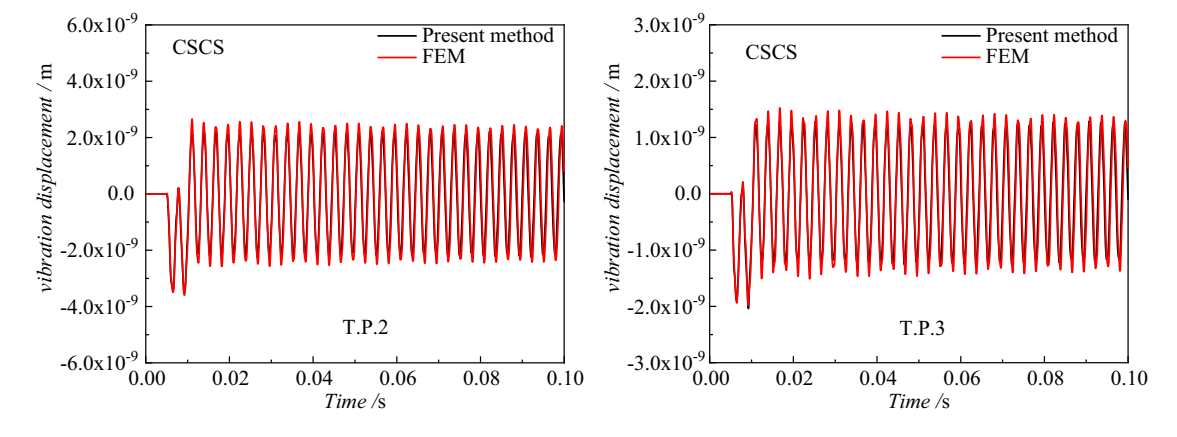


Figure 14: Comparison of the undamped transient vibration response of the present method and FEM.

The displacement response of the sine pulse load and the triangle pulse load is basically the same under SSSS boundary conditions, which is smaller than the displacement response caused by the rectangular pulse load with the passage of time. For CSCS boundary conditions, the response caused by the rectangular pulse load is greater than the response caused by the sine pulse load, while the response caused by the triangular pulse load is the smallest with the passage of time, owing to the amplitude of rectangular pulse load acting on the structure is larger than other loads within a certain period.

For the damped transient vibration response, Figure 17 displays the comparison of the damped transient vibration with different boundary conditions under the rectangular pulse load. The amplitude of the damped vibration response increases with the weakening of the boundary condition. The comparison of the damped

transient vibration with different types of time-dependent loads is shown in Figure 18. Regardless of the boundary condition, the maximum vibration displacement at the initial moment is always caused by the rectangular pulse load, followed by the sine pulse load, and the response caused by the triangle pulse load is the smallest, owing to the amplitude of the rectangular pulse load acting on the structure is larger than other loads within a certain period, which is consistent with the conclusion of the undamped vibration response.

4 Conclusion

In this paper, the unified Jacobi–Ritz method (JRM) is utilized to analyze the dynamic response of the rectangular plate with different boundary conditions. The rec-

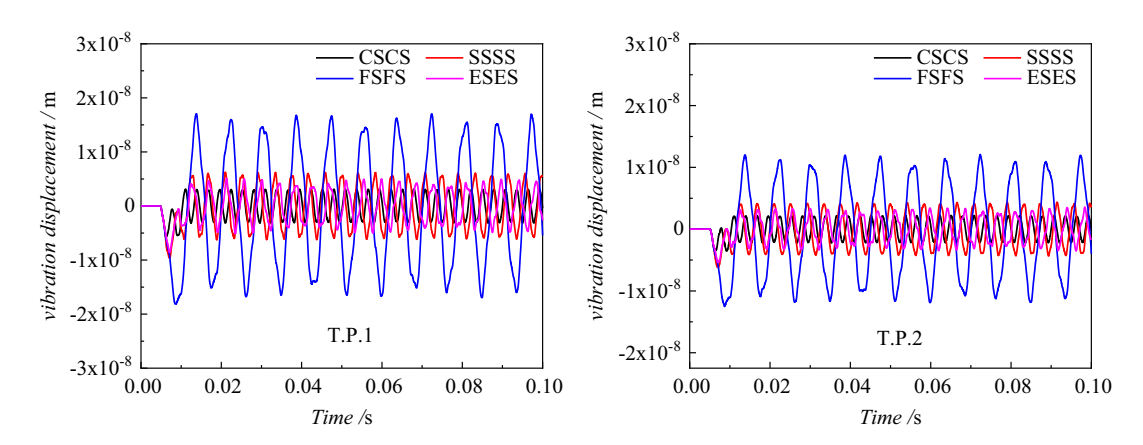


Figure 15: Comparison of the undamped transient vibration with different boundary conditions.

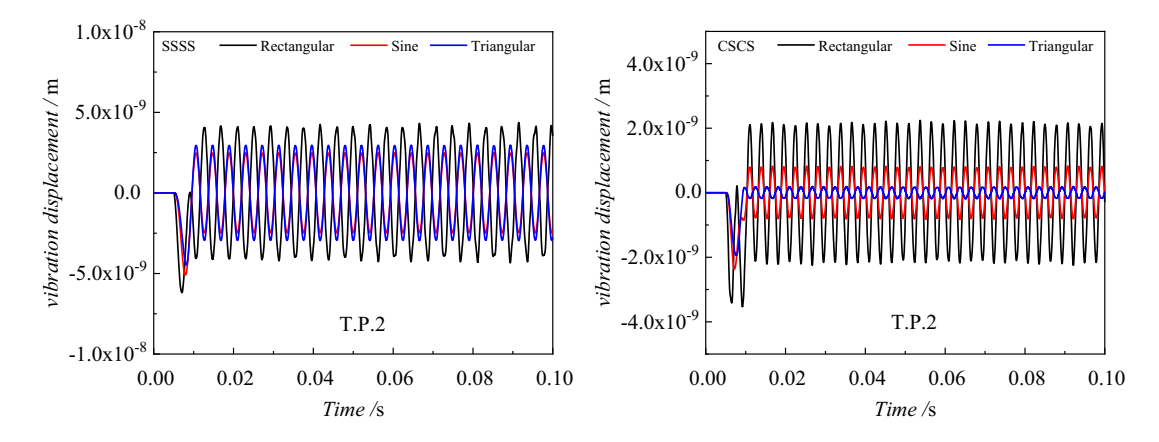


Figure 16: Comparison of the undamped transient vibration with different types of time-dependent loads.

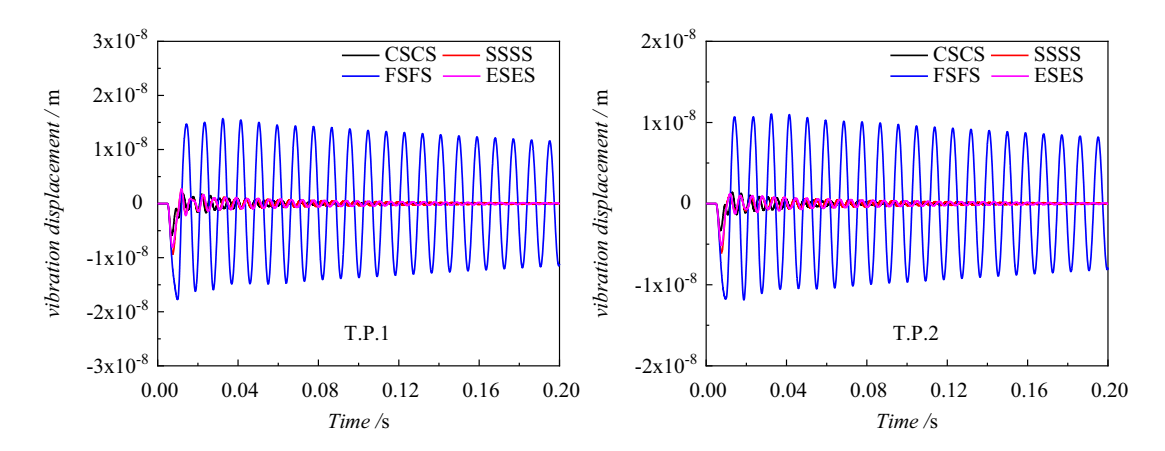


Figure 17: Comparison of the damped transient vibration response with different boundary conditions.

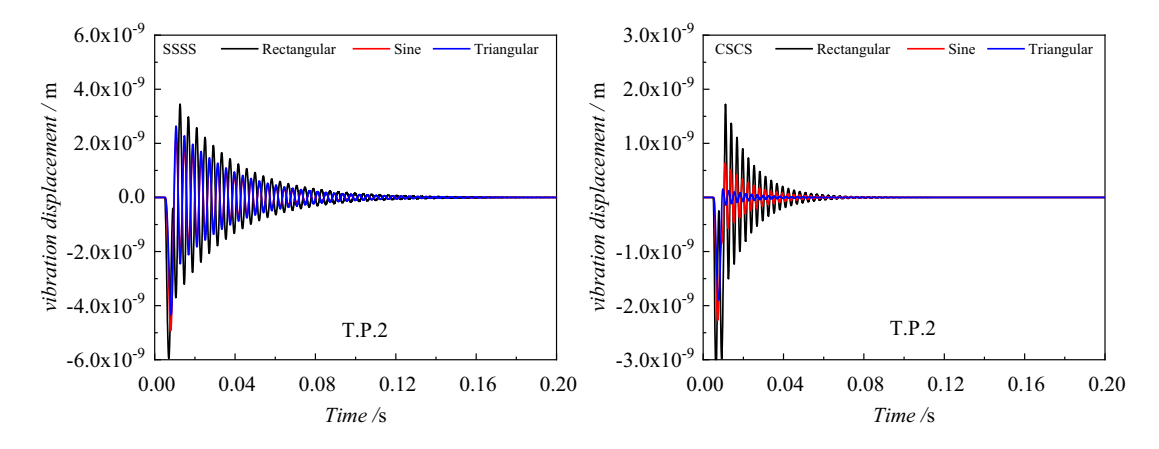


Figure 18: Comparison of the damped transient vibration with different types of time-dependent loads.

tangular plate is divided into several equal sections in the framework of the DDM, and the structural energy functional is established based on the FSDT; five groups of artificial springs are introduced to ensure the continuity of the segments and diversified boundary conditions. The unified Jacobi orthogonal polynomials are expanded to represent the displacement field of the plate in one direction, and the other direction is expressed by the trigonometric series. Polynomials such as Legendre and Chebyshev are special forms of Jacobi polynomial; in other words, the introduction of Jacobi polynomials enriches the selection and diversity of displacement functions.

The free, steady, and transient vibration characteristics of the rectangular plate have been well analyzed by utilizing the Rayleigh–Ritz method, in which the Newmark- β integration method is adopted to realize the time-domain solutions for transient vibration response, especially for the damped transient vibration response, as well as the good convergence and feasibility of the present method have been proved. The effectiveness of

the proposed method is verified by comparing it with the existing literature and FEM results.

The calculation results of the vibration characteristics for the rectangular plate under different boundary conditions, structural scale parameters, and load types are given, indicating that the constraint conditions and geometric dimensions have a significant impact on the dynamic response of the rectangular plate. The results of the study can support the vibration control of the plate structure and further enrich the research data of the JRM.

Acknowledgments: This research was supported by Harbin Engineering University and Naval Research Institute.

Funding information: This study was funded by the National Natural Science Foundation of China (U2006229, 52101351), Ph.D. Student Research and Innovation Fund of the Fundamental Research Funds for the Central Universities (3072020GIP0102), and "Quick Response"

Special Project of Harbin Engineering University (3072020CFT0111).

Author Contributions: Di Jia: Writing and Editing. Cong Gao: Methodology and investigation. Yuliang Yang: Editing and Revision. Fuzhen Pang: Conceptualization and Methodology. Haichao Li: Revision. Yuan Du: Validation.

Conflict of interest: The authors declare that there is no conflict of interest regarding the publication of this paper.

Data availability statement: The data used to support the findings of this study are included within the article.

References

- Kolarevic, N., M. Nefovska-Danilovic, and M. Petronijevic. Dynamic stiffness elements for free vibration analysis of rectangular Mindlin plate assemblies. Journal of Sound & Vibration, Vol. 359, 2015, pp. 84-106.
- Kirisik, R. and S. Yueksel. Free vibration analysis of a rectan-[2] gular plate with Kelvin type boundary conditions. Shock & Vibration, Vol. 14, No. 6, 2013, pp. 447-457.
- Gupta, A. K. and P. Singhal. Thermal effect on free vibration of non-homogeneous orthotropic visco-elastic rectangular plate of parabolically varying thickness. Applied Mathematics, Vol. 1, No. 6, 2010, pp. 456-463.
- Su, X., E. Bai, and A. Chen. Symplectic superposition solution of free vibration of fully clamped orthotropic rectangular thin plate on two-parameter elastic foundation. International Journal of Structural Stability and Dynamics, Vol. 21, No. 9, 2021, id. 2150122.
- Li, H., F. Pang, H. Chen, and Y. Du. Vibration analysis of functionally graded porous cylindrical shell with arbitrary boundary restraints by using a semi analytical method. Composites Part B: Engineering, Vol. 164, 2019, pp. 249–264.
- [6] Du, Y., D. Jia, H. Li, C. Gao, and H. Wang. A unified method to analyze free and forced vibration of stiffened plates under various edge conditions. European Journal of Mechanics a-Solids, Vol. 94, 2022, id. 104573.
- Qin, Z., F. Chu, and J. Zu. Free vibrations of cylindrical shells with arbitrary boundary conditions: a comparison study. International Journal of Mechanical Sciences, Vol. 133, 2017, pp. 91-99.
- Liu, Y., Z. Qin, and F. Chu. Nonlinear forced vibrations of FGM sandwich cylindrical shells with porosities on an elastic substrate. Nonlinear Dynamics, Vol. 104, No. 2, 2021, pp. 1007-1021.
- Shi, D., H. Zhang, Q. Wang, and S. Zha. Free and forced vibration of the moderately thick laminated composite rectangular plate on various elastic winkler and pasternak foundations. Shock and Vibration, Vol. 2017, No. PT.4, 2017, pp. 1-23.
- [10] Javani M., Y. Kiani, and M.R. Eslami. Application of generalized differential quadrature element method to free vibration of FG-

- GPLRC T-shaped plates. Engineering Structures, Vol. 242, 2021, id. 112510.
- [11] Huang, J., Y. Tang, H. Li, F. Pang, and Y. Qin. Vibration characteristics analysis of composite floating rafts for marine structure based on modal superposition theory. Reviews on Advanced Materials Science, Vol. 60, No. 1, 2021, pp. 719-730.
- Gao, C., H. Zhang, H. Li, F. Pang, and H. Wang. Numerical and experimental investigation of vibro-acoustic characteristics of a submerged stiffened cylindrical shell excited by a mechanical force. Ocean Engineering, Vol. 249, 2022, id. 110913.
- Yang, J., J. Liu, and J. Li. Analysis of a rectangular ceramic plate in electrically forced thickness-twist vibration as a piezoelectric transformer. IEEE Transactions on Ultrasonics, Ferroelectrics and Frequency Control, Vol. 54, No. 4, 2007, pp. 830-835.
- [14] Akbarov, S. D., N. Yahnioglu, and U. B. Yesil. 3D analysis of the forced vibration of a prestressed rectangular composite platewith two neighboring cylindrical cavities. Computers Materials & Continua, Vol. 28, No. 2, 2012, pp. 147-164.
- [15] Wu, C. F., S. H. Liu, and Y. J. Chen. Applying the principle of mixed variables solve the problems of forced vibration of the calculating rectangular plate by uniform load. Applied Mechanics & Materials, Vol. 71-78, 2011, pp. 1715-1719.
- [16] Fan, Z. The effects of viscoelastic boundary supports on the forced vibration of a rectangular plate. Journal of Vibration Engineering, Vol. 14, 2001, pp. 183-186.
- Xiao, Y. G. and C. P. Yang. Free vibration analysis for disconnected thin rectangular plate with four free edges on nonlinear elastic foundation. Applied Mechanics & Materials, Vol. 52-54, 2011, pp. 1309-1314.
- [18] Xiao, Y. G., C. P. Yang, and H. Hu. Nonlinear forced vibration analysis for thin rectangular plate on nonlinear elastic foundation. Applied Mechanics & Materials, Vol. 204-208, 2013, pp. 4716-4721.
- [19] Zhong, Z., Y. Xiao, and C. Yang. Nonlinear forced vibration analysis for thin rectangular plate on nonlinear elastic foundation. Research Journal of Applied Sciences, Engineering and Technology, Vol. 5, No. 9, 2013, pp. 2163-2167.
- [20] Zhang, C. L., W. Q. Chen, and J. S. Yang. Electrically forced vibration of a rectangular piezoelectric plate of monoclinic crystals. International Journal of Applied Electromagnetics & Mechanics, Vol. 31, No. 4, 2009, pp. 207-218.
- [21] Nasirshoaibi, M. and N. Mohammadi. Forced transverse vibration analysis of an elastically connected rectangular double-plate system with a Pasternak middle layer. ARPN Journal of Engineering and Applied Sciences, Vol. 10, No. 14, 2015, pp. 6004-6013.
- [22] Wang, Q., D. Shi, Q. Liang, and F. Pang. Free vibration of fourparameter functionally graded moderately thick doubly-curved panels and shells of revolution with general boundary conditions. Applied Mathematical Modelling, Vol. 42, 2017, pp. 705-734.
- [23] Wang, Q., X. Cui, B. Qin, Q. Liang, and J. Tang. A semi-analytical method for vibration analysis of functionally graded (FG) sandwich doubly-curved panels and shells of revolution. International Journal of Mechanical Sciences, Vol. 134, 2017, pp. 479-499.
- [24] Agarana, M. C. and A. I. Ehigbochie. Forced vibration numerical analysis of rectangular elastic orthotropic damped inclined mindlin plate using finite difference algorithm. Applied Mathematics, Vol. 9, No. 6, 2018, pp. 618-632.

- [25] Yahnioglu, N. and U. B. Yesil. Forced vibration of an initial stressed rectangular composite thick plate with a cylindrical hole. *ASME International Mechanical Engineering Congress & Exposition*, Vol. 15, 2009, pp. 337–343.
- [26] Ju-Hai, M. A. The method of mixed variables for solving the problems of forced vibration of the rectangular plate under uniform load. World Earthquake Engineering, Vol. 23, No. 3, 2007, pp. 158–162.
- [27] Chen, X., L. Chen, S. Huang, M. Li, and X. Li. Nonlinear forced vibration of in-plane bi-directional functionally graded materials rectangular plate with global and localized geometrical imperfections – ScienceDirect. Applied Mathematical Modelling, Vol. 93, 2021, pp. 443–466.
- [28] Kim, S. M. Influence of horizontal resistance at plate bottom on vibration of plates on elastic foundation under moving loads. *Engineering Structures*, Vol. 26, No. 4, 2004, pp. 519–529.
- [29] Niu Y, and M. Yao. Linear and nonlinear vibrations of graphene platelet reinforced composite tapered plates and cylindrical panels. Aerospace Science and Technology, Vol. 115, 2021, id. 106798.
- [30] Yang, Y., B. Chen, W. Lin, Y. Li, and Y. Dong. Vibration and symmetric thermal buckling of asymmetric annular sandwich plates with piezoelectric/GPLRC layers rested on foundation. *Aerospace Science and Technology*, Vol. 110, 2021, id. 106495.
- [31] Gunasekaran, V., J. Pitchaimani, and L. Chinnapandi. Vibroacoustics response of an isotropic plate under non-uniform edge loading: An analytical investigation. *Aerospace Science* and Technology, Vol. 105, 2020, id. 106052.
- [32] Ou, D. and C. M. Mak. Transient vibration and sound radiation of a stiffened plate. *Journal of Vibration and Control*, Vol. 19, No. 9, 2013, pp. 1378-1385.
- [33] Fan, Z. Transient vibration and sound radiation of a rectangular plate with viscoelastic boundary supports. *International Journal for Numerical Methods in Engineering*, Vol. 51, No. 5, 2001, pp. 619–630.
- [34] Geng, L., X. Zhang, Y. Zhang, and L. Xu. Reconstruction of transient vibration and sound radiation of an impacted plate [C]//INTER-NOISE and NOISE-CON Congress and Conference Proceedings. *Institute of Noise Control Engineering*, Vol. 253, No. 6, 2016, pp. 2288–2295.
- [35] Geng, L., X. Z. Zhang, and C. X. Bi. Reconstruction of transient vibration and sound radiation of an impacted plate using time domain plane wave superposition method. *Journal of Sound & Vibration*, Vol. 344, 2015, pp. 114–125.
- [36] He, G. and M. Kashiwagi. Nonlinear solution for vibration of vertical plate and transient waves generated by wave impact. *International Journal of Offshore & Polar Engineering*, Vol. 19, No. 19, 2009, pp. 189–197.
- [37] Sheikh, A. H. and M. Mukhopadhyay. Linear and nonlinear transient vibration analysis of stiffened plate structures. *Finite Elements in Analysis and Design*, Vol. 38, No. 6, 2002, pp. 477–502.

- [38] Hajheidari, H. and H. R. Mirdamadi. Free and transient vibration analysis of an un-symmetric cross-ply laminated plate by spectral finite elements. *Acta Mechanica*, Vol. 223, No. 11, 2012, pp. 2477–2492.
- [39] Skočilas, J., B. Skočilasová, and J. Soukup. Determination of the rheological properties of thin plate under transient vibration. *Latin American Journal of Solids & Structures*, Vol. 10, No. 1, 2013, pp. 189-195.
- [40] Pang, F., Y. Qin, H. Li, Y. Teng, Q. Gong, and S. Wang. Study on impact resistance of composite rocket launcher. *Reviews on Advanced Materials Science*, Vol. 60, No. 1, 2021, pp. 615-630.
- [41] Pang, F., H. Li, H. Chen, and Y. Shan. Free vibration analysis of combined composite laminated cylindrical and spherical shells with arbitrary boundary conditions. *Mechanics of Advanced Materials and Structures*, Vol. 28, No. 2, 2021, pp. 182–199.
- [42] Gao, C., F. Pang, H. Li, and L. Li. An approximate solution for vibrations of uniform and stepped functionally graded spherical cap based on Ritz method. *Composite Structures*, Vol. 233, 2020, id. 111640.
- [43] Li, H., F. Pang, X. Miao, and Y. Li. Jacobi-Ritz method for free vibration analysis of uniform and stepped circular cylindrical shells with arbitrary boundary conditions: A unified formulation. Computers & Mathematics with Applications, Vol. 77, No. 7, 2019, pp. 427-440.
- [44] Gao, C., F. Pang, H. Li, H. Wang, J. Cui, and J. Huang. Free and forced vibration characteristics analysis of a multispan timoshenko beam based on the Ritz method. *Shock and Vibration*, Vol. 2021, 2021, id. 4440250. (WOS: 000683141400004).
- [45] Du, Y., F. Pang, L. Sun, and H. Li. A unified formulation for dynamic behavior analysis of spherical cap with uniform and stepped thickness distribution under different edge constraints. *Thin-Walled Structures*, Vol. 146, 2020, id. 106445.
- [46] Gao, C., F. Pang, H. Li, D. Jia, and Y. Tang. Steady and transient vibration analysis of uniform and stepped annular/circular plates based on FSDT. *Acta Mechanica*, Vol. 233, No. 3, 2022, pp. 1061–1082.
- [47] Su, Z., G. Jin, and T. Ye. Free vibration analysis of moderately thick functionally graded open shells with general boundary conditions. *Composite Structures*, Vol. 117, 2014, pp. 169–186.
- [48] Shi, Z., X. Yao, F. Pang, and Q. Wang. An exact solution for the free-vibration analysis of functionally graded carbon-nanotube-reinforced composite beams with arbitrary boundary conditions. Scientific reports, Vol. 7, No. 1, 2017, id. 12909.
- [49] Qin, Z., Z. Yang, J. Zu, and F. Chu. Free vibration analysis of rotating cylindrical shells coupled with moderately thick annular plates. *International Journal of Mechanical Sciences*, Vol. 142, 2018, pp. 127–139.
- [50] Ilanko, S., L. Monterrubio, and Y. Mochida. The Rayleigh-Ritz method for structural analysis. John Wiley & Sons, 2014.
- [51] Xing Y, and B. Liu. Closed form solutions for free vibrations of rectangular Mindlin plates[J]. Acta Mechanica Sinica, Vol. 25, No. 5, 2009, pp. 689-698.